# Proximitized Josephson junctions in highly-doped InAs nanowires robust to optical illumination

**IOP ebooks**™

Bringing together innovative digital publishing with leading authors from the global scientific community.

Start exploring the collection−download the first chapter of every title for free.

# Proximitized Josephson junctions in highly-doped InAs nanowires robust to optical illumination

Lily Yang[1] , Stephan Steinhauer[1] , Elia Strambini[2], Thomas Lettner[1],
Lucas Schweickert[1], Marijn A M Versteegh[1] , Valentina Zannier[2] ,
Lucia Sorba[2] , Dmitry Solenov[3] and Francesco Giazotto[2]

[1] Department of Applied Physics, KTH Royal Institute of Technology, Albanova University Centre, SE-106 91 Stockholm, Sweden
[2] NEST, Istituto Nanoscienze-CNR and Scuola Normale Superiore, Piazza S. Silvestro 12, Pisa I-56127, Italy
[3] Department of Physics, Saint Louis University, St. Louis, MO 63103, United States of America

E-mail: lilyy@kth.se

## Abstract

We have studied the effects of optical-frequency light on proximitized InAs/Al Josephson junctions based on highly $n$-doped InAs nanowires at varying incident photon flux and at three different photon wavelengths. The experimentally obtained $IV$ curves were modeled using a resistively shunted junction model which takes scattering at the contact interfaces into account. Despite the fact that the InAs weak link is photosensitive, the Josephson junctions were found to be surprisingly robust, interacting with the incident radiation only through heating, whereas above the critical current our devices showed non-thermal effects resulting from photon exposure. Our work indicates that Josephson junctions based on highly-doped InAs nanowires can be integrated in close proximity to photonic circuits. The results also suggest that such junctions can be used for optical-frequency photon detection through thermal processes by measuring a shift in critical current.

Supplementary material for this article is available online

(Some figures may appear in colour only in the online journal)

## 1. Introduction

Semiconductor–superconductor hybrid devices have attracted increasing attention in state-of-the-art quantum information processing. The interaction of these devices with electromagnetic radiation in the optical domain opens up exciting opportunities for both emerging technologies and fundamental science. Several optoelectronic device architectures have been proposed including entangled-photon pair sources [1, 2], Josephson lasers [3], and photonic Bell-state analyzers [4]. Experimentally, enhanced photon generation in light-emitting diodes based on conventional epitaxially-grown semiconductor $p$–$n$ junctions contacted by superconducting leads have been demonstrated [5]. Semiconducting nanowires constitute an important building block for devices relying on superconducting electrodes and the proximity effect [6–9]. Such hybrid devices have been shown for a variety of material systems, such as InAs [10] or InSb [11] nanowires covered with epitaxial Al, InAs nanowires with Pb [12] and Nb [13] contacts, InSb nanowires contacted by NbTiN leads [14], InN nanowire-Nb junctions [15], PbS nanowires with

PbIn electrodes [16] and CdTe–HgTe core–shell nanowires in combination with Al contacts [17]. Surprisingly, the fundamental transport characteristics of proximitized nanowire junctions interacting with photons at optical wavelengths have remained unexplored despite the significant technological importance of the related phenomena, for instance in devices interfacing superconductors with optics [18]. The realization of large-scale quantum networks requires the combination of quantum hardware nodes and photonic platforms compatible with fiber-based telecommunication [19], necessitating coherent interfaces between photons and qubits similar to those proposed for superconducting devices [20], trapped ions [21], and solid-state spins [22, 23].

Optical wavelength photons can have a significant effect on the superconductivity in hybrid superconductor–semiconductor Josephson junctions. Early experiments on light-sensitive semiconductor–superconductor junctions showed that CdS thin films between Pb or Sn electrodes could be switched to a Josephson state related to a persistent conductivity enhancement [24]. Furthermore, the interface barrier [25] and the critical current [26] of superconducting junctions on two-dimensional electron gases could be adjusted by light exposure. More recently, non-equilibrium effects of photo-excited carriers in graphene-based Josephson junctions have been reported [27]. In particular, the electrical transport in low-bandgap semiconductors such as InAs has been shown to be highly responsive to light [28], bringing to question whether hybrid superconducting devices based on such semiconductors can be operated in close proximity to photonic elements.

In this work, we present a comprehensive study on the electrical transport properties of highly *n*-doped InAs nanowires proximitized by superconducting Al electrodes during exposure to light inside a dilution refrigerator. The nanowire Josephson junctions were exposed to laser illumination in the visible and infrared range, in particular at three wavelengths: 532 nm, 790 nm (around Rb transitions relevant for atomic quantum memories) and 1550 nm (C-band telecommunication window). Experiments were performed at increasing incident photon flux and the obtained results were modeled using a shunted junction model that accounts for scattering at the semiconductor–superconductor interfaces. Using an independently measured temperature-dependent data set, the *IV* characteristics were fitted to distinguish between thermal and non-thermal effects. Our results demonstrate the Josephson junctions' robustness to optical photon exposure, establishing a parameter window suitable for operating semiconductor-based Josephson junctions under optical light illumination, which is, for instance, relevant for their integration with quantum photonic circuits.

# 2. Methods

## 2.1. Sample fabrication

Se-doped InAs nanowires were grown by Au-assisted chemical beam epitaxy [29]. The n-type nanowires have an average diameter of 80nm and a length of 2.6 $\mu$m. The typical electron concentration of the nanowires is $n \approx 2 \times 10^{18}$ cm$^{-3}$ with a mobility of $\mu \approx 1200$ cm$^2$ V$^{-1}$ s$^{-1}$ and a mean free path of 30 nm, estimated from transconductance characterization at $T = 4$ K on similar nanowires [30]. The nanowire-based InAs/Al Josephson junction devices were fabricated using the following steps: substrates of Si with 150 nm thermal oxide were pre-patterned with Au alignment markers using electron beam lithography, evaporation, and lift-off. Next, the highly *n*-doped InAs nanowires were spun-cast on the pre-patterned substrates and imaged by scanning electron microscopy (SEM) to determine their precise locations and orientations relative to the alignment markers. Contact electrodes and bonding pads were aligned to the randomly positioned nanowires using the SEM images of the nanowires and their adjacent alignment markers. A second electron beam lithography step was performed on a bi-layer PMMA resist (approximately 200 nm for each layer) by a Raith Voyager system (50 kV electron acceleration voltage). Automatic alignment procedures were employed to ensure precise positioning of the Al electrodes on the InAs nanowires. After resist development the samples were first cleaned with a mild oxygen plasma for 15 s to remove residual resist. The plasma was kept short to avoid additionally oxidizing the nanowire surface. Next, the sample was loaded into an AJA Orion magnetron sputtering tool. The native oxide layer on the nanowire surfaces was removed *in situ* with Ar ions in a physical plasma etching process (15 mTorr, 45 W RF power, 3 min excluding power ramping). Subsequently, an Al layer of 100 nm was deposited at 150 W RF power and 3 mTorr Ar pressure. To facilitate lift-off, the sample holder was not rotated during the deposition. After deposition, the samples were immersed in standard resist remover at room temperature. The majority of the Al is then mechanically removed from the surface by tweezers, and ultrasonication in a clean beaker of remover at room temperature was employed to complete lift-off. Figure 1(a) shows an SEM image of a representative device.

## 2.2. Transport measurements

The electrical transport properties were characterized in a Bluefors dilution refrigerator with a base temperature around 10 mK. The InAs/Al Josephson junction devices were wire-bonded to ceramic chip packages and mounted on the mixing chamber stage, being electrically connected to thermally anchored low-pass RC filters. Two RC filters were connected in series for each electrical line. Outside the dilution refrigerator, the electrical lines were filtered with pi-filters at room temperature. *IV* measurements were performed in a four-point configuration with a customized battery-powered instrument (*IVVI* rack developed at TU Delft) for current biasing and voltage readout. The experiments under light illumination employed commercially available optical components (ThorLabs) and continuous-wave laser sources at the three investigated wavelengths.
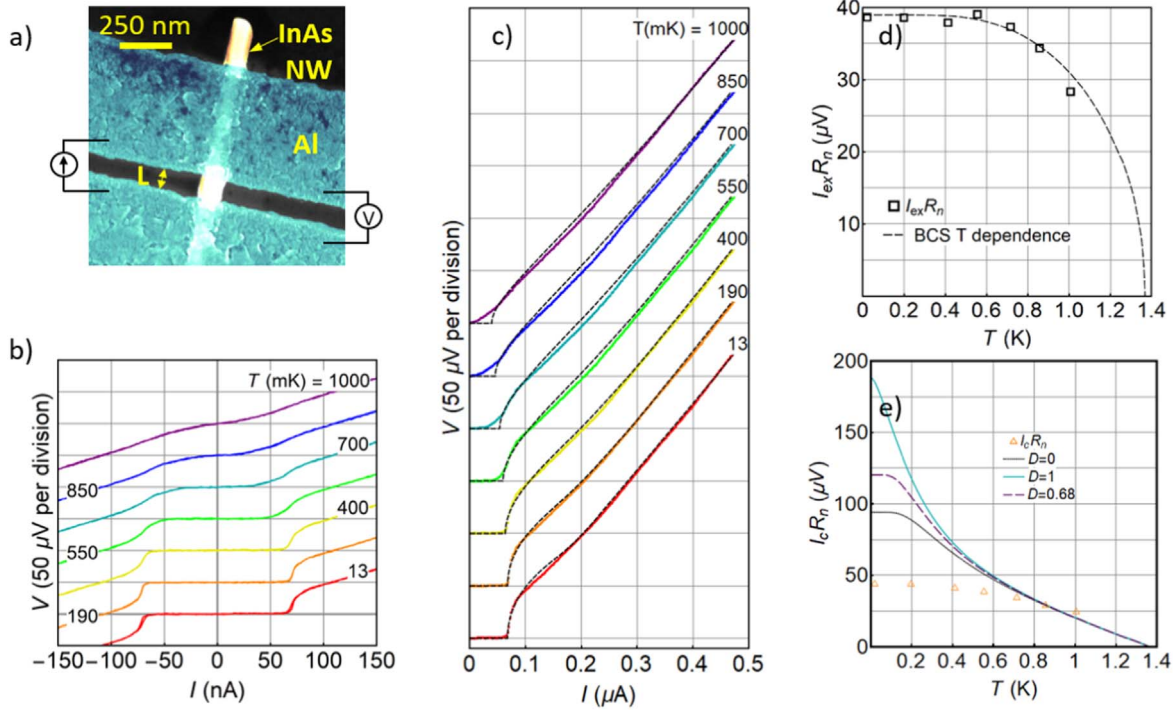
**Figure 1.** (a) Scanning electron microscopy image of n-doped InAs nanowire contacted by two Al leads separated by a gap $L$ of approximately 100 nm. The four-point measurement configuration is schematically indicated. (b) *IV* characteristics obtained under DC current biasing at different cryostat temperatures (the sample was not exposed to photons during the measurements). Curves are vertically offset by 50 $\mu$V for clarity. (c) Experimental data fitted to a shunted junction model (black lines). Curves are vertically offset by 50 $\mu$V for clarity. (d) The product of excess current times normal state resistance $I_{ex}R_n$ extracted from the model shows good agreement with a BCS-type temperature dependence. (e) Experimental data (orange triangle) and three theoretical curves based on an analytical formula for ballistic junctions [31]. The limiting cases of $D = 0$ and $D = 1$, as well as an intermediate transmission coefficient of $D = 0.68$ (corresponding to the value extracted by fitting our data, as discussed below), are shown, all deviating from experimental observations, corroborating the diffusive transport characteristics in the presented devices.

## 3. Results

The InAs nanowires were contacted by two Al leads separated by a gap $L$ of approximately 100 nm (figure 1(a)), which forms the Josephson junction. The leads were used for both current biasing and voltage measurements in a four-point configuration. The transport characteristics were first measured as a function of temperature without photon exposure by heating the sample stage in the dilution refrigerator. The experimentally obtained *IV* curves (figure 1(b)) show a gradual suppression of proximity-induced superconductivity in the InAs nanowire with increasing temperature. The slightly rounded transitions between the superconducting and the normal state without hysteresis are consistent with previous studies of InAs nanowire Josephson junctions with medium contact transparency [32]; a more detailed discussion on the junction transparency will be presented below. As is often seen in this type of junctions, the normal region of the *IV* curves is linear but shifted from the normal state line given by Ohm's law [33]. By fitting the linear region ($V > 2\Delta$) in our data and extrapolating the fit to the $V = 0$ axis (figure 1(c)), we obtain the normal state resistance $R_n$ and an excess current $I_{ex}$. The excess current arises from Andreev reflections and depends on the junction transparency $D$ and the superconducting gap $\Delta(T)$. Since the superconductivity in the nanowire is induced by the Al contacts, we expect $I_{ex}R_n(T)$ to follow BCS temperature dependence, which is verified in figure 1(d). Furthermore, we expect the junctions to be in the diffusive regime because the mean free path is shorter than the junction length, which was corroborated by comparing our data with a model for a ballistic junction. This model could not reproduce the experimental data for a range of junction transparencies, as shown in figure 1(e).

The *IV* curves were analyzed in two steps. First, we applied a 1D Boltzmann-equation approach [33] to model the *IV* curves taken at different temperatures without laser illumination. The junction was modeled as two S–N interfaces, each represented by a repulsive potential $H\delta(x)$, which represents the effect of the typical oxide layers and any disorder and defects found at the interfaces. To simplify the formulas we introduce the dimensionless parameter $Z = \hbar v_F H\delta(x)$, where $\hbar$ is the reduced Planck's constant and $v_F$ the Fermi velocity. $Z$ is related to the interface transmission coefficient $D$ through the equation $D = 1/(1 + Z^2)$. Charge carriers in the semiconductor link are divided into two populations according to their direction of travel. The current through the device at each point is described by

$$I = 2\,e\,\rho(0)\,v_F\,S \int_{-\infty}^{\infty} d\epsilon\,[f_{\rightarrow}(\epsilon) - f_{\leftarrow}(\epsilon)], \qquad (1)$$

where $\rho(0)$ is the density of states at zero temperature, $S$ is a geometric factor, $f_{\leftarrow/\rightarrow}(\epsilon)$ is the distribution function of

charge carriers moving left or right, and energy $\epsilon$ is measured from the local chemical potential. The current through the device was calculated by matching boundary conditions at each interface and applying energy considerations. Since significant scattering is expected in our nanowire junctions, we assumed the distribution of quasiparticles to be thermal within the semiconducting nanowire, consistent with non-ballistic transport. In such a diffusive junction, a normal conducting channel exists in parallel with the superconducting channel. Therefore, the total current through the junction includes both a superconducting term and a normal conducting term

$$I = I_c \sin \phi + I_n(V), \tag{2}$$

where $I_c$ denotes the magnitude of the supercurrent, $I_n$ the current due to quasiparticle transport, and $\frac{d\phi}{dt} = \frac{2e}{h}V(t)$. Since $V \sim d\phi/dt$, the observed time-averaged potential difference as a function of current can be obtained by inverting equation (2) and integrating over a full period in $\phi$:

$$\frac{1}{\langle V \rangle} = \frac{1}{2\pi}\int_0^{2\pi} \frac{d\phi}{V_n(\phi)} = \frac{1}{2\pi}\int_0^{2\pi} \frac{d\phi}{V_n(I - I_c \sin\phi)}. \tag{3}$$

By solving equation (1) self-consistently and using the inverted equation (3), we fitted our experimental *IV* curves with four key parameters: the critical current $I_c(T)$, the normal state resistance $R_n(T)$, the transmission coefficient $D$, and the effective superconducting gap of the Al leads at the interface $\Delta(T)$. The experimental data is well described by fitting such a model (figure 1(c)) except for the sub-gap region, where thermal contributions not included in the theoretical framework are observed. The fitting was done iteratively as follows: To reduce the number of adjustable parameters per fit, we first extracted the normal state resistance $R_n(T)$ as well as the excess current $I_{ex}(T)$ from each *IV* curve by fitting the region $V > 2\Delta(T)$, in this case $V > 125\,\mu V$, with $V = (I - I_{ex})R_n$. Now we are left with three adjustable parameters: $I_c(T)$, $Z$, and $\Delta(T)$. Note that $\Delta(T)$ is proportional to $I_{ex}(T)R_n(T)$ and follows BCS dependence, as shown in figure 1(d). Therefore, only the temperature-independent parameter $\Delta_0 = \Delta(T = 0)$ was needed. Furthermore, $Z$ was also assumed to be independent of temperature [33]. Therefore, of the three adjustable parameters, only $I_c(T)$ is temperature dependent. We fit the entire series of *IV* curves iteratively, where $I_c(T)$ was adjusted when fitting each of the *IV* curves obtained for different temperatures, while the $Z$ and $\Delta_0$ were fixed for all temperatures but adjusted over multiple fitting iterations. Generally, we obtained better agreement with the experimental curves assuming that one interface is dominating, contributing most of the observed voltage drop. In a similar manner, InAs nanowire Josephson junctions with significant disorder were previously described by a model relying on a lumped scatterer with single effective transparency [34]. Non-identical InAs/Al interfaces could also be explained by slight doping gradients along the nanowire axis or differences resulting from the nanofabrication process.

For the presented device, we obtained a transmission coefficient of 0.68 and $\Delta_0 = 60\,\mu eV$. Note that the gap energy

is substantially smaller compared to the Al leads (208 $\mu$eV), which were measured independently. This behavior can be attributed to the inverse proximity effect and significant spin–orbit interaction in the nanowire material suppressing superconductivity, consistent with previous observations in similar devices [35]. The medium interface transparency of 0.68 can be attributed to the physical plasma etching employed *in situ* before Al deposition, potentially inducing disorder and scattering at the interfaces [36]. Our nanofabrication procedure did not include a commonly used sulfur-based surface treatment [37]; the physical etching approach was adopted due to its reliability, uniformity and reproducibility (five out of five nanowire junctions tested at cryogenic temperatures showed proximity-induced superconductivity; see the supplementary data available online at stacks.iop.org/NANO/32/075001/mmedia). Diffusive transport through the nanowire can be verified by comparing the product $I_c(T)R_n(T)$ with ballistic temperature dependence curves [31] corresponding to different transmission coefficient values $D$ for comparison (figure 1(e)). Clearly, $I_c(T)R_n(T)$ cannot be fitted with a ballistic transport model for Josephson junctions, confirming that the quasiparticle channel is diffusive.

The impact of photon exposure on the Josephson junction properties was studied under illumination for three different wavelengths using an optical setup inside the dilution refrigerator (figure 2(a)). Optical fibers delivered the photons from three independent laser sources to the sample stage, where they were out-coupled to free space, collimated, and directed onto the same position on the nanowire sample (only one laser was used at a time). The measured beam profile gave a Gaussian beam radius of 1.6 mm, considerably larger than the devices under test. The transport properties of the nanowire Josephson junctions under constant current bias were characterized while the junctions were exposed to photons with wavelengths of 532 nm, 790 nm, and 1550 nm at increasing impinging laser power. Representative *IV* curves are shown in figure 2(b) in comparison to the sample stage heating experiment. The annotated effective temperatures were extracted using a fitting procedure detailed below. The behavior for the sub-gap region of the *IV* curve at $V < 2\Delta$ was qualitatively similar for all four cases: proximity-induced superconductivity was gradually suppressed with increasing impinging laser power (temperature) and the *IV* curves began to adopt more linear Ohmic characteristics similar to the effect of heating. This is more clearly illustrated by color maps of the derivative $dV/dI$ (figure 2(c)).

To quantitatively link the experimental results under photon exposure with the heating experiment, the sub-gap region of the *IV* curve ($V < 2\Delta$) was fitted with temperature as the only adjustable parameter. This was accomplished by first interpolating between the data points from the temperature experiment to arrive at an experimentally determined fitting function $V(I, T)$. Then, each of the *IV* curves under laser illumination was fitted with this empirically obtained $V(I, T)$. This empirical fit accounts for all thermally activated processes. Two exemplary fitting results for each wavelength are presented in figures 3(a)–(c). In the sub-gap region, the fit
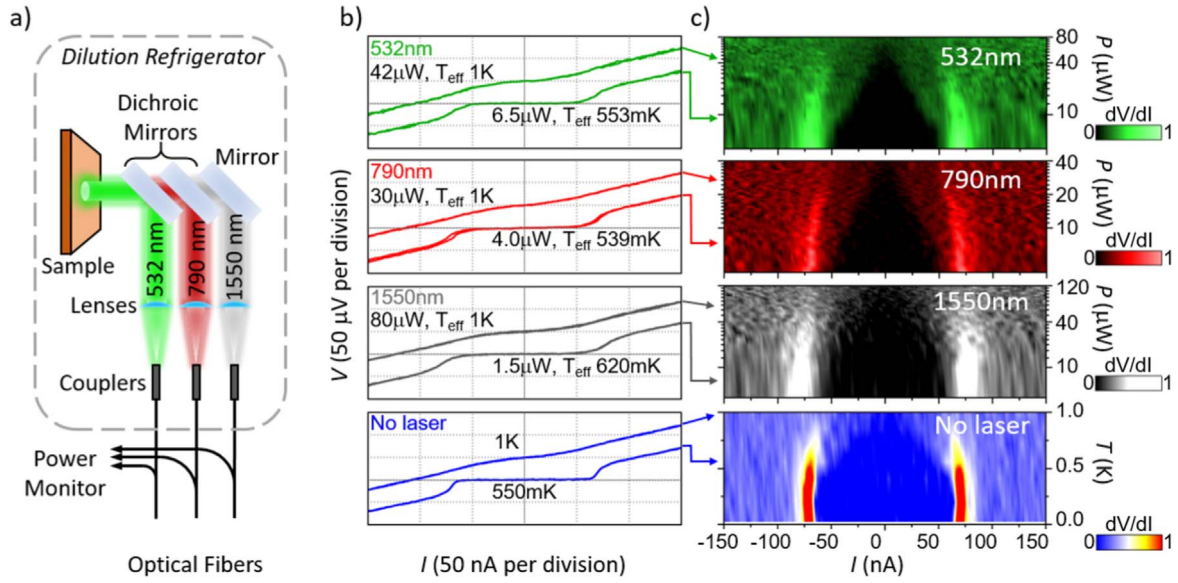
**Figure 2.** (a) Schematics of the experimental configuration used to characterize nanowire Josephson junctions under illumination. (b) Three top graphs: *IV* curves at selected impinging laser powers corresponding to effective temperatures around ~540–620 mK and 1 K for three different wavelengths. Bottom graph: *IV* curves obtained during sample stage heating experiments under no external illumination for comparison. (c) *dV/dI* as a function of current bias showing the suppression of proximity-induced superconductivity for increasing impinging laser powers and sample stage temperatures.
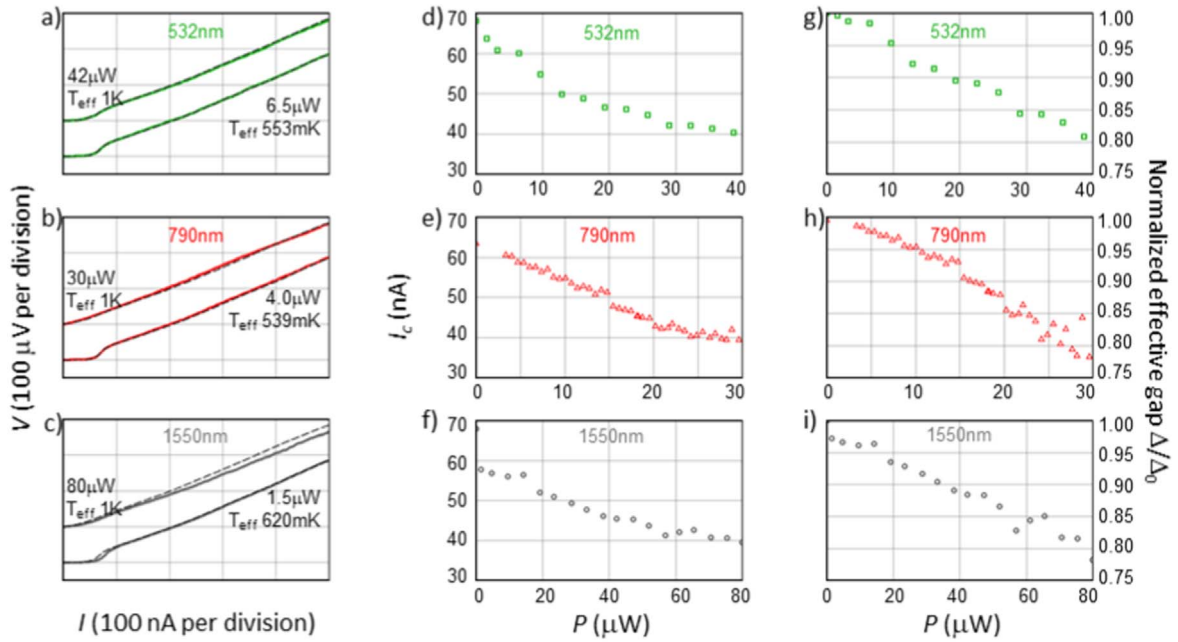


**Figure 3.** (a)–(c) *IV* curves at selected laser powers for three different wavelengths fitted with interpolated data obtained in sample stage heating experiments with no external illumination (dashed lines). The interpolated data was computed from *IV* curves recorded at different temperatures and was used to extract the effective temperature from the fit model. (d)–(f) The critical current $I_c$ deduced from the fit as a function of laser power. (g)–(i) The effective gap normalized to the value at base temperature under no laser illumination.

provided by the interpolation is in excellent agreement with experimental data, showing that laser illumination of the sample is equivalent to heating as far as the Josephson physics is concerned, and no new observable features are introduced. Additionally, we verified that the Al leads remained superconducting for the optical input powers presented here, and therefore aggravates the heating similar to previous experiments reported in the literature [38].

Having established that the sub-gap region can be modeled using temperature as the only variable, we assign an effective temperature $T_{eff}$ to each *IV* curve under illumination. $T_{eff}$ obtained from this procedure was then used in the model above to extract the critical current $I_c$ (figures 3(d)–(f)) and the superconducting gap at the interface between the superconductor and the semiconductor (figures 3(g)–(i)), as well as to establish a reliable relation between local sample
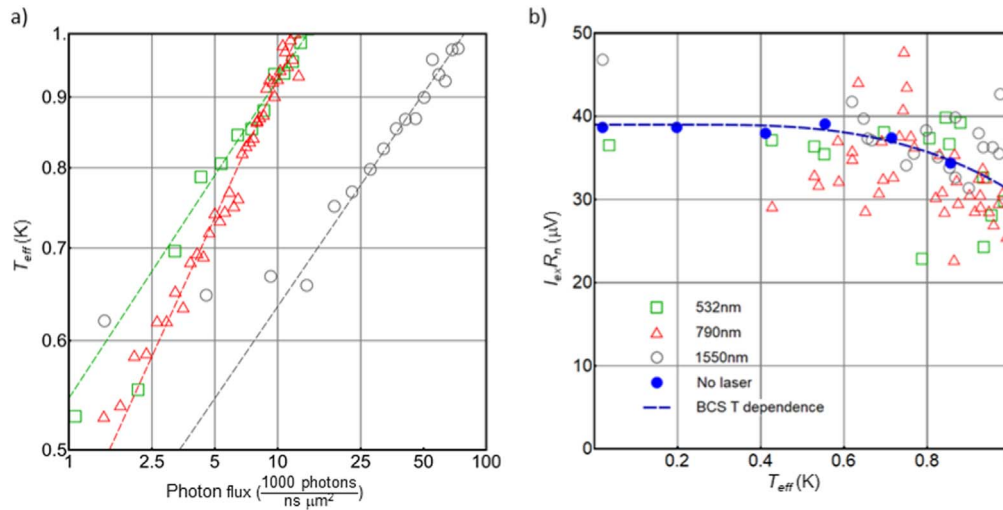
**Figure 4.** (a) Effective temperature $T_{eff}$ as a function of impinging photon flux for the three laser wavelengths. Dotted lines are guides to the eye. (b) The product of excess current times normal state resistance $I_{ex}R_n$ as a function of effective temperature $T_{eff}$ for laser illumination at three different wavelengths and increasing sample stage temperatures (filled blue circles). BCS dependence (dashed line) describes the temperature data. Non-monotonous deviations from BCS dependence were observed under photon exposure in contrast to the case of sample stage heating.

temperature and the laser power for each wavelength. To establish a window of operation for the hybrid Josephson junction under optical illumination, we compare $T_{eff}$ to the number of impinging photons $N$ in figure 4(a). Three trend lines have been superimposed on the data showing $T_{eff} \sim N^{1/a}$ and are intended as guides to the eye. Characteristic exponents $a$ of 4.3, 3.0, and 4.53 were found for 532 nm, 790 nm, and 1550 nm, respectively. The observed differences for the three wavelengths are attributed to an interplay of varying absorption in the InAs nanowire, the Al leads, and the Si substrate.

In contrast to the sub-gap region, the region of the *IV* curves above the gap, $V > 2\Delta$, does change under illumination. The power dependence there is non-monotonic and does not map to any effective temperature dependence (see figure 4(b)). It is surprising that, while the excess current $I_{ex}$, the normal state resistance $R_n$ and the combination $I_{ex}R_n$ exhibit similar non-monotonic changes with laser power, Josephson tunneling responsible for the superconducting plateau and $I_c$ appear to be unaffected by photon exposure, except via local temperature. This invites further theoretical investigation of the self-shunted Josephson systems under illumination. Non-thermal effects in the normal state resistance under laser illumination can be attributed to the electron density affected by the number of absorbed photons, and to interface defects in the system interacting with the incident light. The complex fluctuation-like behavior is analogous to previous experimental observations on nanowire Josephson junctions under external gate voltage [13].

## 4. Conclusion

In conclusion, highly-doped InAs nanowire junctions are robust to illumination by optical photons; the effect of the

incident photons on the Josephson physics can be effectively described by only varying the device temperature. On the other hand, the normal conducting part of the *IV* curves shows non-monotonous behavior that cannot be modeled using temperature alone. The effective superconducting gap observed in these hybrid junctions begins to close as the effective temperature reaches approximately 0.6 K, corresponding to the incoming photon density of approximately $2 \times 10^{19}$– $4 \times 10^{19}$ photons per second in the laser beam, or 2000–5000 photons per ns per $\mu m^2$. Our results indicate a window in which a hybrid, highly-doped InAs nanowire Josephson junction can be operated as an integral part of future hybrid superconducting optoelectronic circuits, especially when supported by appropriate thermal management measures.

## ORCID iDs

Lily Yang  https://orcid.org/0000-0002-5011-9320
Stephan Steinhauer  https://orcid.org/0000-0001-6875-6849
Marijn A M Versteegh  https://orcid.org/0000-0001-6659-9237

Valentina Zannier ⓘ https://orcid.org/0000-0002-9709-5207
Lucia Sorba ⓘ https://orcid.org/0000-0001-6242-9417

## References

[1] Recher P, Nazarov Y V and Kouwenhoven L P 2010 *Phys. Rev. Lett.* **104** 156802
[2] Hayat A, Kee H Y, Burch K S and Steinberg A M 2014 *Phys. Rev. B* **89** 094508
[3] Godschalk F, Hassler F and Nazarov Y V 2011 *Phys. Rev. Lett.* **107** 073901
[4] Sabag E, Bouscher S, Marjieh R and Hayat A 2017 *Phys. Rev. B* **95** 094503
[5] Sasakura H *et al* 2011 *Phys. Rev. Lett.* **107** 157403
[6] Doh Y J, van Dam J A, Roest A L, Bakkers E P A M, Kouwenhoven L P and De Franceschi S 2005 *Science* **309** 272–5
[7] Giazotto F, Spathis P, Roddaro S, Biswas S, Taddei F, Governale M and Sorba L 2011 *Nat. Phys.* **7** 857–61
[8] de Lange G, van Heck B, Bruno A, van Woerkom D J, Geresdi A, Plissard S R, Bakkers E P A M, Akhmerov A R and DiCarlo L 2015 *Phys. Rev. Lett.* **115** 127002
[9] Lutchyn R M, Bakkers E P A M, Kouwenhoven L P, Krogstrup P, Marcus C M and Oreg Y 2018 *Nat. Rev. Mater.* **3** 52–68
[10] Deng M T, Vaitiekenas S, Hansen E B, Danon J, Leijnse M, Flensberg K, Nygård J, Krogstrup P and Marcus C M 2016 *Science* **354** 1557–62
[11] Zhang H *et al* 2018 *Nature* **556** 74–9
[12] Paajaste J, Amado M, Roddaro S, Bergeret F S, Ercolani D, Sorba L and Giazotto F 2015 *Nano Lett.* **15** 1803–8
[13] Günel H Y, Batov I E, Hardtdegen H, Sladek K, Winden A, Weis K, Panaitov G, Grützmacher D and Schäpers T 2012 *J. Appl. Phys.* **112** 034316
[14] Zhang H *et al* 2017 *Nat. Commun.* **8** 16025
[15] Frielinghaus R, Batov I E, Weides M, Kohlstedt H, Calarco R and Schäpers T 2010 *Appl. Phys. Lett.* **96** 132504
[16] Kim B K, Kim H S, Yang Y, Peng X, Yu D and Doh Y J 2017 *ACS Nano* **11** 221–6
[17] Hajer J, Kessel M, Brüne C, Stehno M P, Buhmann H and Molenkamp L W 2019 *Nano Lett.* **19** 4078–82
[18] De Franceschi S, Kouwenhoven L, Schönenberger C and Wernsdorfer W 2010 *Nat. Nanotechnol.* **5** 703–11
[19] Wehner S, Elkouss D and Hanson R 2018 *Science* **362** eaam9288
[20] Andrews R W, Peterson R W, Purdy T P, Cicak K, Simmonds R W, Regal C A and Lehnert K W 2014 *Nat. Phys.* **10** 321–6
[21] Mehta K K, Bruzewicz C D, McConnell R, Ram R J, Sage J M and Chiaverini J 2016 *Nat. Nanotechnol.* **11** 1066–70
[22] Gao W B, Imamoglu A, Bernien H and Hanson R 2015 *Nat. Photon.* **9** 363–73
[23] Awschalom D D, Hanson R, Wrachtrup J and Zhou B B 2018 *Nat. Photon.* **12** 516–27
[24] Giaever I 1968 *Phys. Rev. Lett.* **21** 1286–9
[25] Akazaki T, Hashiba H, Yamaguchi M, Tsumura K, Nomura S and Takayanagi H 2009 *J. Phys.: Conf. Ser.* **150** 052004
[26] Schäpers T, Müller R P, Kaluza A, Hardtdegen H and Lüth H 1999 *Appl. Phys. Lett.* **75** 391–3
[27] Tsumura K, Furukawa N, Ito H, Watanabe E, Tsuya D and Takayanagi H 2016 *Appl. Phys. Lett.* **108** 033109
[28] Fang H *et al* 2016 *Nano Lett.* **16** 6416–24
[29] Gomes U, Ercolani D, Zannier V, Beltram F and Sorba L 2015 *Semicond. Sci. Technol.* **30** 115012
[30] Iorio A, Rocci M, Bours L, Carrega M, Zannier V, Sorba L, Roddaro S, Giazotto F and Strambini E 2019 *Nano Lett* **19** 652
[31] Kuprianov M Y and Lukichev V 1988 *Sov. Phys.—JETP* **67** 1163
[32] Gharavi K 2017 *Nanotechnology* **28** 085202
[33] Blonder G E, Tinkham M and Klapwijk T M 1982 *Phys. Rev. B* **25** 4515
[34] Abay S, Persson D, Nilsson H, Wu F, Xu H Q, Fogelström M, Shumeiko V and Delsing P 2014 *Phys. Rev. B* **89** 214508
[35] Tiira J, Strambini E, Amado M, Roddaro S, San-Jose P, Aguado R, Bergeret F, Ercolani D, Sorba L and Giazotto F 2017 *Nat. Commun.* **8** 14984
[36] Gul O *et al* 2017 *Nano Lett.* **17** 2690–6
[37] Suyatin D B, Thelander C, Bjork M T, Maximov I and Samuelson L 2007 *Nanotechnology* **18** 105307
[38] Singh M and Chan M 2013 *Phys. Rev. B* **88** 064511